Max H2 DR

Maximise H2 Enrichment in Direct Reduction Shaft Furnaces

Digital demonstration of granular particle movement and gas flow by coupled DEM/CFD simulations

Deliverable D2.2 by WP2. Partners: RUB, BFI, M26

RUB: Klidi Qyteti, Enric Illana Mahiques, Viktor Scherer

BFI: Thomas Piontek, Yalcin Kaymak, Kersten Marx, Thorsten Hauck

RUHR UNIVERSITÄT BOCHUM RUB

BFI

July 2024

This project has received funding from the European Union under grant agreement NUMBER — 101058429 — MaxH2DR

Table of contents

List of Figures

List of Tables

1. Introduction

The focus of this deliverable can be summarized as a digital demonstration of granular particle movement and gas flow by coupled DEM/CFD simulations – The computations by the DEM/CFD model will be validated against some selected physical demonstration experiments. This is the content of the current report.

> Deliverable 2.2 is fulfilled and documented in this report. Selected experiments have been compared against DEM/CFD simulations. The comparison between BFI and RUB experiments and RUB simulations revealed minor differences in pressure values and pressure drop gradients, suggesting variations in parameters such as local porosity field.
>
> This first step of digital demonstration of particle and gas flow will be continued in deliverable D1.4 to consider also reactions and will be finalised in deliverable D2.3 considering all available results including the cold demonstration-scale trials at BFI and the hot shear cell results of UniSA.

Three experimental setups were utilized: a simple shaft geometry of LEAT and two test rigs from BFI, a tubular device and a shaft construction. The LEAT shaft and BFI tubular device, characterized by their vertical orientation and simple flow direction, were used for preliminary tests. The BFI shaft construction is more complex, allowing for adjustments in the angle of the side panels and equipped with two inlets for gas flow. The comparison between LEAT and BFI experiments and RUB simulations revealed minor differences in pressure values and pressure drop gradients, suggesting variations in parameters such as local porosity field.
The numerical simulations foreseen in WP2 employ the in-house DEM-CFD code from RUB [1, 2], being developed in a larger project (BULK-REACTION) funded by the German Science Foundation. It provides advanced open-source libraries applicable to reacting moving granular assemblies passed by reactive gas flows. In contrast to other implementations, which are restricted to spherical particles only, the software allows for arbitrarily shaped moving objects (defined by their triangulated surfaces) [3] with varying size and shape over time [4]. The in-house code at RUB has already been used for the simulation of rotary kilns, lime shaft kilns and also for the simulation of processes in blast furnaces [5, 6].

While the basic programming work and the numerical development are objectives of the abovementioned project, the required adaption and application to the industrial DRI-process are the goals pursued within WP2 of MaxH2DR. Basically, the new advanced code is able to compute the movement and thermochemical interaction of large assemblies of reacting particles (Lagrangian description of particle movement) with a simultaneously passing gas, while considering all additional transport equations (continuous Navier-Stokes & scalar transport of species and enthalpy) required to describe gas-phase reaction. The coupling between both phases determines the interstitial flow-field evolution in terms of pressure drop as well as species distribution and transport processes at the solid-fluid interface.

To reasonably limit the required computational effort while preserving the capability of addressing large-scale industrial devices, the high geometrical resolution must be restricted to those regions where gradients are steep (e.g., fluid inlets, locus of mechanical agitation, reaction zones) while approximating the remaining domain with a less demanding approach. Further background references (radiation, reaction) and explanations may be found in [2].

2. Experimental setups and simulation methods

2.1 Experimental setups at the BFI

A Midrex shaft-furnace-type test facility (Figure 1, middle) was built to analyze the interaction of particles and gas flow. To determine the gas permeability of the sample material, additional tests were done in a simple tubular device (Figure 1, left).

The tubular device has a simple shape with a well-defined flow direction of gas (air) and particles. The tube is positioned vertically and filled up with the material. A slide with a sieve is placed inside the tube to keep the material at a specific height. In Figure 1, the CAD-Sketch is shown (left). The diameter of the tube is 300 mm and the filling height is 1400 mm. The air flows upwards. The outlet for the counter flow of the solids is at the bottom.

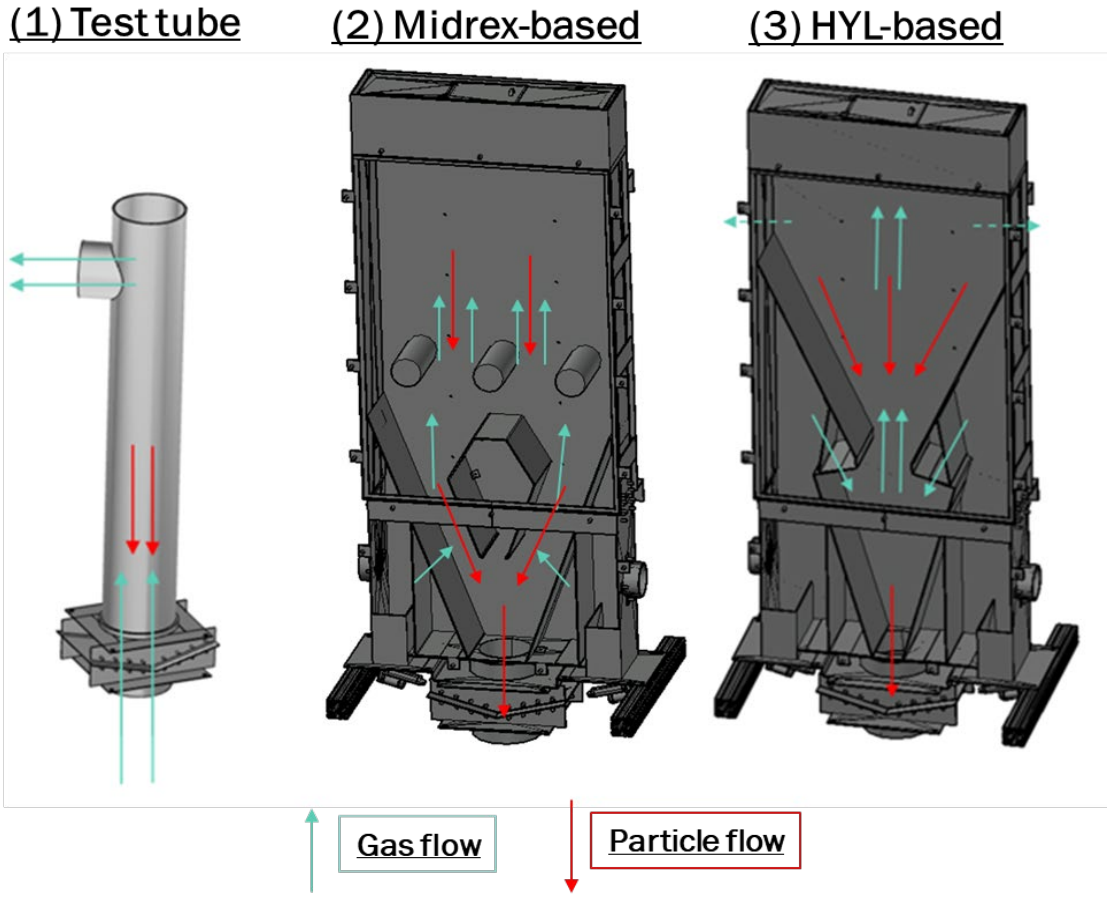

Figure 1: CAD sketches. Left: tubular device, middle: Midrex-based shaft construction, right: HYL-based shaft construction

The shaft constructions in Figure 1 (middle and right) are quasi-two-dimensional with a rectangular base. The dimensions are 2900x1200x300 mm. The setup has two inlets for the gas (air). The flow is directed upwards to the outlet at the top. The mass flow of the solids is directed downwards and leaves the test rig through an outlet at the bottom. The installations inside are exchangeable. The pressure drops are measured for different sections and the material flow is recorded with a camera through the acrylic front plate and analyzed with MATLAB. Depending on the setting of the slide gates and the ventilator, various operating conditions are adjustable.

For the shaft construction, a minimum bulk volume of 0.8 m^3 is needed. To neglect boundary effects, the particle size has to be smaller than 20 mm.

The distributions of particle size and particle shape were determined using continuous image evaluation methods. These quantities are measured again after a certain number of tests since particle wear occurs at regular intervals. The two distributions have a significant influence on the bulk porosity as well as a pressure drop in the bulk, which directly changes the force transmission between gas and bulk flow. Measurements are made with the so-called "Camsizer", shown in Figure 2, which is based on the principle of static image analysis. This device from Retsch Technology can analyze and evaluate particles from 20 µm - 30 mm.

Figure 2: Camsizer for the determination of particle size and shape distribution

2.2 Experimental setup at RUB

As experimental results from Task 2.1 were not yet available at the project onset, experimental data available from a generic counterflow configuration were used (see Figure 3). The objective was to verify the correct reproduction of momentum exchange between the particles (which determines the solid outflow rates) and with the counter-flowing fluid phase (which establishes a measurable pressure drop and reduces or even prevents the outflow).

The experimental setup is sketched in Figure 3 (a). It consists of a flat bottom silo geometry with a narrow inlet channel at the bottom attached to it. The main silo chamber has a horizontal cross section of 400 mm x 100 mm and a height H = 580 mm. At the bottom center an orifice of width W_{in} = 102 mm is located, which has a height of H_{in} = 40 mm. A photograph of the experimental setup is shown in Figure 3 (b), where the silo is filled with dodecahedra.

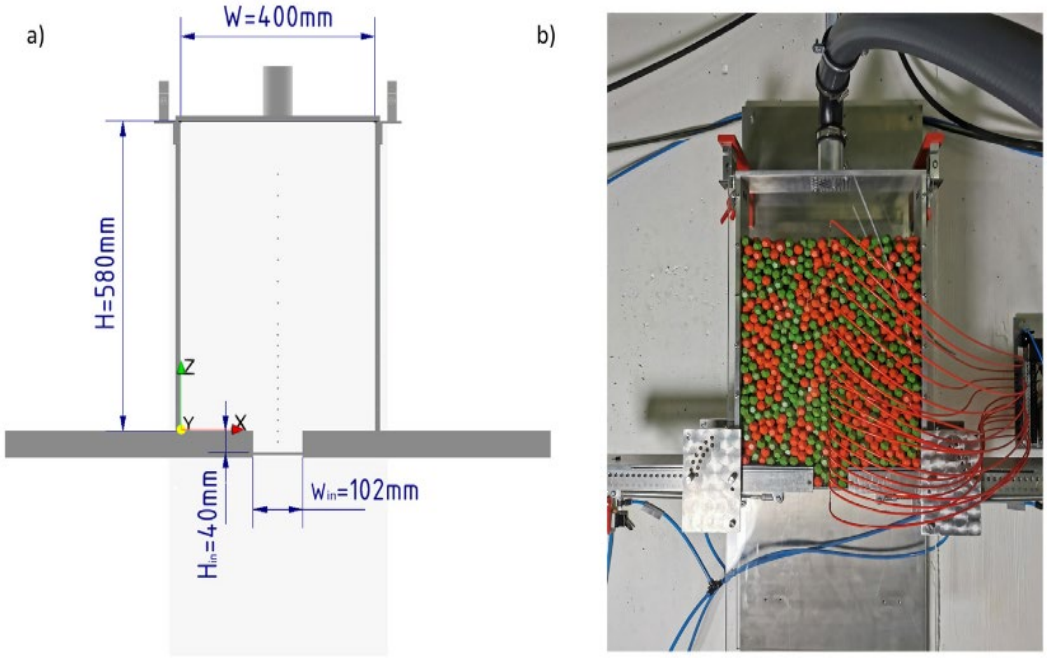

Figure 3: Sketch of hopper geometry (a) & Experimental setup filled with dodecahedra (b) – test facility at RUB

Pressure is measured in the test rig at the centerline of the silo. Measurements were carried out with spherical wood particles of 10 mm diameter. The diameter corresponds to the experiments with the wooden pellets done by UniSA as part of Task 1.2 and described in detail in Deliverable 1.2. Note that measurements with dodecahedra have been carried out too. Within this report, only the results for the spherical particles are shown.

2.3 DEM-CFD Method

The DEM-CFD coupling routines available combine the Discrete Element Method (DEM) with Computational Fluid Dynamics (CFD), creating a dual simulation framework. When fluids and bulk solids flow together, both the homogeneous fluid and the discrete solid particles experience intense dynamic interaction. If these processes occur at vastly different timescales, the slower one can be treated as steady state. This allows for calculation of the faster process in a time-dependent manner for a sequence of these static states. For instance, if the blockage of the fluid domain by the solid particles as a "porous medium" that is stationary for a short period is considered, this coupled Stokes flow (for fluids) and Darcy flow (for porous media) problem can be solved using modified incompressible Navier-Stokes equations. These equations incorporate additional, spatially-dependent frictional forces arising from the bulk material [7]. However, it is crucial to choose a sufficiently small time step interval for the Navier-Stokes equations. During this interval, the solid phase is assumed stationary. This ensures that the time evolution of porosity due to fluid interaction is captured accurately. This calculation method also permits complex particle shapes in the simulation, which allow for irregularly shaped polyhedra as model bodies.

The DEM component describes the particle motion of each individual particle, including the forces and contacts between them and any surrounding walls. It essentially solves simplified versions of Newton's laws of motion (for movement) and Euler's equations (for rotation) for every particle, all in real-time. If only contact forces are considered in simplified form, the forms of the equations of motion shown in equations (1) and (2) result. In the case of a simultaneous gas flow, the drag forces formed by the relative velocity must be added to these sums.

$$m_i \frac{d^2\vec{x}_i}{dt^2} = \sum_{j=1}^{n_{K,i}} \vec{F}_{ij} + m_i \cdot \vec{g} \tag{1}$$

$$\theta_i \frac{d^2\vec{\varphi}_i}{dt^2} = \sum_{j=1}^{n_{K,i}} \vec{M}_{ij} = \sum_{j=1}^{n_{K,i}} \vec{r}_j \times \vec{F}_{ij} \tag{2}$$

where $d^2\vec{x}_i/dt^2$ is the acceleration, $d^2\vec{\varphi}_i/dt^2$ is the angular acceleration, m_i is the mass and θ_i is the moment of inertia of the particle i. $\vec{F}_{ij}$ and $\vec{M}_{ij}$ are the force and moment resulting from contact with particles.

Lagrange tracking is employed to follow the motion of solid objects, thus also requiring an accurate representation of particle geometry, interaction and dynamics. This goes beyond mere spherical contact resolution as its capabilities must include reaction and energy transport within the particles themselves. For situations involving a flowing gas phase, DEM considers the local porosity of the particle bed to determine the forces or momentum transfer between the two phases over time. As the particles move and their orientation changes, DEM continuously updates the porosity, affecting how the fluid flows through the gaps. This feature enhances the fidelity of simulations, capturing the intricate details of particle behavior and internal processes.

On the CFD side, the routine leverages the capabilities of OpenFOAM, a computational fluid dynamics platform. It excels in simulating fluid flow, as well as the transport of energy (enthalpy and thermal radiation) and species within the fluid domain. The integration of OpenFOAM enhances the applicability of fluid dynamics simulations for the intended use, providing an understanding of the complex interplay between simultaneously moving and reacting fluid and solid phases.

The code is fully parallelized on the CFD and DEM side in order to limit the computing times despite the unavoidable large computational effort. The coupling of the two software packages leads to DEM/CFD, where the two programs exchange data such as bulk material porosity and particle-resolved momentum transfer (from DEM to CFD) or gas phase velocity and flow resistance (from CFD to DEM).

3. Results

The results chapter is structured as follows: First, the experimental results of the generic counterflow configuration (Figure 3) available are compared against initial coupled DEM/CFD simulations. Second, the experiments for the tubular test rig (Figure 1.1) at BFI is presented and compared against DEM/CFD simulations. Third, simulations of the Midrex configuration (Figure 1, middle) are presented. Corresponding experiments are ongoing at BFI.

3.1 Comparison of RUB experiments in a generic counter flow configuration and initial coupled DEM/CFD simulations

DEM/CFD simulations were carried out for the experimental configuration shown in Figure 3. The inflow of air through an orifice into the hopper of the silo model is investigated for volume flow rates of 100 and 200 m^3/h, leading to superficial velocities at the inlet of 2.72 and 5.45 m/s, respectively.

The RUB DEM/CFD code is employed for the numerical simulation of the gas flow through the hopper. Pressure-velocity coupling is solved using the PISO method. A constant inlet velocity is specified at the bottom of the hopper based on the desired volume flow rate. Inflow turbulence is set to a turbulence intensity of 5%.

The orifice is located at z = 0. The majority of the pressure drop is occurring at the inlet region due to the locally high velocity. Downstream of the orifice, the pressure decreases mainly due to the drag of the particles. The experimental runs are shown with error bars for standard deviation (red). Two available pressure drop descriptions for spherical particles, the classical "Ergun" correlation and the "diFelice" model, successfully replicated the observed pressure drop in the silo outflow.

The Ergun equation is an empirical equation that describes the pressure drop in a packed bed or fluidized bed system[1]. The equation takes the form of:

$$\Delta P = [(150\ \mu_F\ (1-\varepsilon_f)^2\ \vec{u}_f) / d^2\ \varepsilon_f^3]\ L + [(1.75\ (1-\varepsilon_f)\ \rho_f\ \vec{u}_f^2 L) / d\ \varepsilon_f^3] \quad (3)$$

where ΔP is the pressure drop across the bed, μ_F is the dynamic viscosity of the fluid, ρ_f is the density of the fluid, ε_f is the void fraction of the bed (the fraction of the bed volume that is not occupied by solid particles), $\vec{u}_f$ is the superficial velocity of the fluid, d is the diameter of the particles, and L is the bed length.

The first term on the right-hand side of the equation represents the frictional (laminar) pressure drop due to the resistance of the fluid flow through the bed and it is proportional to the viscosity, the superficial velocity and the inverse square of the particle diameter. The second term on the right-hand side of the equation represents the pressure drop caused by the inertial of the flow (turbulent) with respect to the particles and, thus, it is proportional to the square of the superficial velocity and the length of the bed. Both terms include the effect of the void fraction, which is the most relevant variable of the model.

[1] http://faculty.washington.edu/finlayso/Fluidized_Bed/FBR_Fluid_Mech/packed_beds_fbr.htm

The diFelice model is a correlation of experimental data for calculating pressure drop in packed beds of spherical particles. The drag force on a particle in a fluid-multiparticle interaction system is expressed as:

$$\vec{f}_d = 1/2\ \varepsilon_f^2\ C_d\ \rho_f A_\perp\ u_f{}^2\ \varepsilon_f^{-\chi} \quad (4)$$

Where $\vec{f}_d$ is the drag force, ε_f is the bed porosity, C_d is the drag coefficient, ρ_f is the fluid density, u_f is the fluid velocity, χ is an empirical factor and $A_\perp$ is the projected area of the particle in direction of the fluid flow [7]. Subsequently, the pressure drop is calculated as:

$$\Delta P = 1/2\ \varepsilon_f^2\ C_d\ (L/d)\ \rho_f\ u_f{}^2\ \varepsilon_f^{-\chi} \quad (5)$$

L is the bed length and d the particle diameter. The drag coefficient C_d and the empirical factor χ are defined as follows:

$$C_d = (0.63 + 4.8/\sqrt{Re})^2 \quad (6)$$

$$\chi = 3.7 - 0.65 \exp\left[-\frac{(1.5-\log_{10}(Re))^2}{2}\right] \quad (7)$$

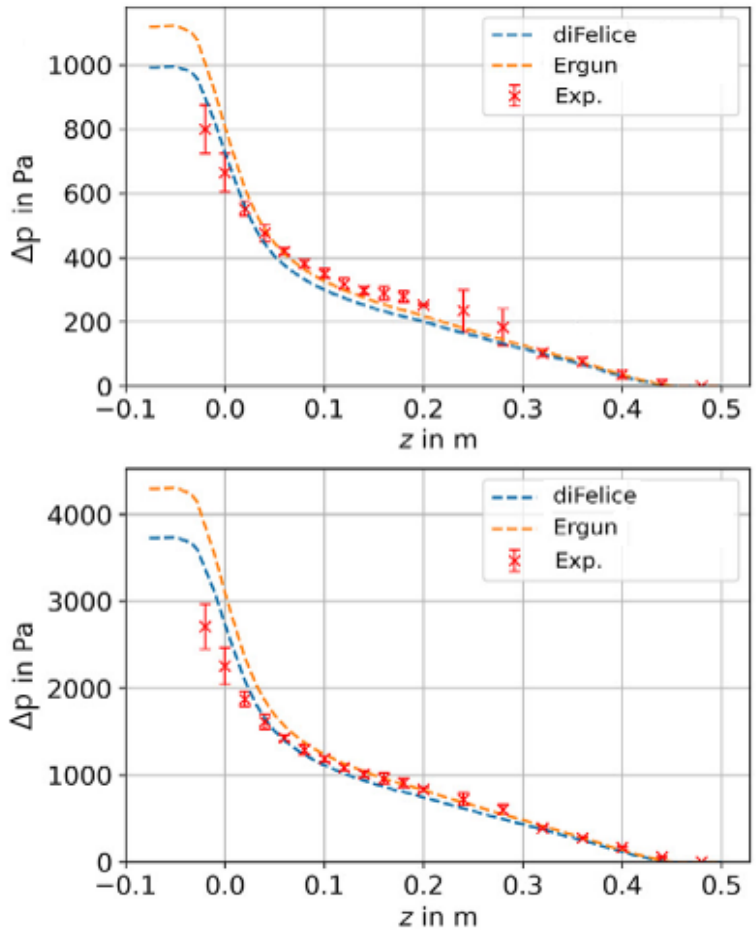

Figure 4: Results for the pressure drop from the experiments with spheres (red), simulations using the diFelice method (blue) and simulations using Ergun equation to calculate the pressure drop (orange) for the volume flow rates of 100 m^3/h (top) and 200 m^3/h (bottom)

The agreement between the simulated and actual pressure drop confirms the effectiveness of these models in predicting granular flow behavior in silos. As is shown in Figure 4 above, the results reveal that the Ergun and diFelice model provide almost identical results. As the Ergun model is a standard in OpenFoam, it has been decided to use the Ergun equation in all further simulations.

3.2 Experiments in the BFI tubular rig and comparison against corresponding DEM/CFD simulations

Before any experiments in the tubular test rig were performed the particle size distribution is analyzed. For the analysis of the particles, a representative sample must be taken first. The particles are stored and delivered in big bags. From these, samples were taken and mixed from different positions of the bulk material, i.e. from above, the respective sides, or by moving the bulk material also below the surface. As mentioned in the previous chapter, shapes and sizes are determined in the measuring device "Camsizer", and the sample quantity is 500-1000 g in each case. The respective distribution curves and sphericity are then calculated from this. The particle volume distribution can be seen in Figure 5.

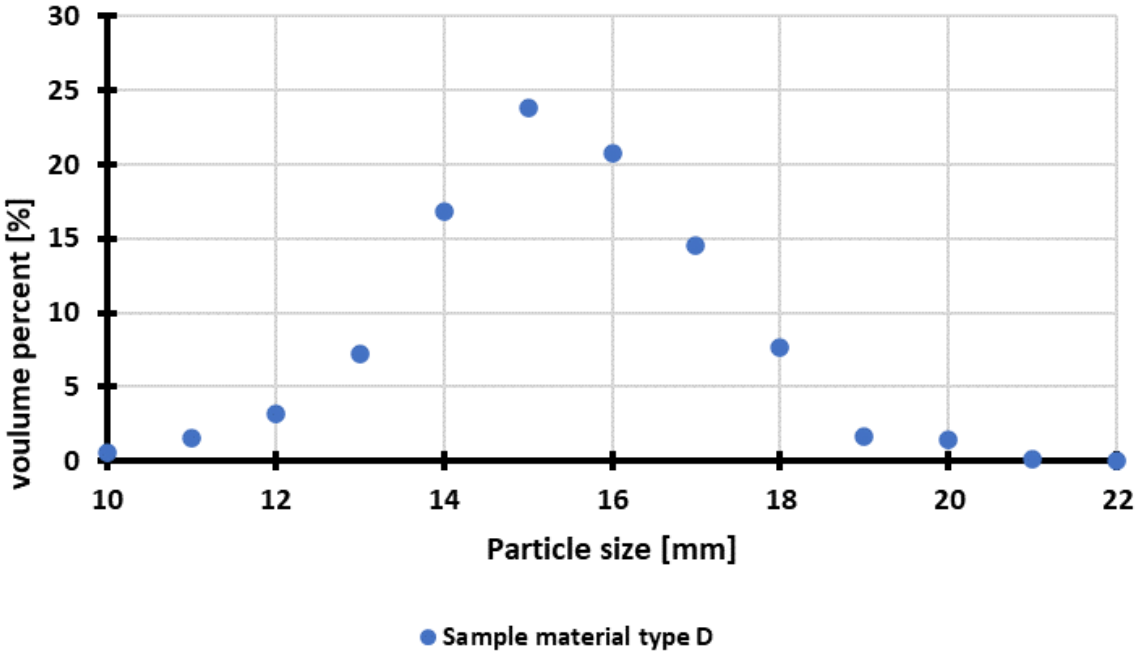

Figure 5: Distribution curve of a particle analysis of the DR-Pellets used

To investigate porosity and bulk density, the volume of the bulk was determined before and after the tests in the test tube. The bulk density and porosity can then be calculated from the density of the material, the mass that has flowed out, and the filling volume. Table 1 shows the analyses of the materials. The D50 diameter of the test material type D (bauxite-coated DR-Pellets) is 14.3 mm. The measured mean sphericity is 0.936, the calculated bulk density is 3768 kg/m^3 and the mean porosity is 0.42. Furthermore, two sample bulks of wooden spheres were used for experiments. They are monodispersed and have a size of 12 mm and 15 mm.

The experiments in the tubular rig were performed with two different experimental methods. The first involves steady-state experiments, which are performed without bulk movement. Airflow is generated from bottom to top. The second method is the so-called dynamic test. Here, a material flow in countercurrent to the airflow is generated via an opening of the slide gates. The particle flow and its influence on the permeability are determined in the process.

Various factory-calibrated measuring devices are used which are compiled in Table 1.

Sensor	***Measured variable***	***Measuring range***	***Measurement accuracy***
CTV 210-R Kimo	Gas velocity	0-30 m/s	±3 % from the measured value ±0.03 m/s
DDM/2 Titec	Differential pressure	adjustable: max. 0-70 mbar	setting-dependent: 0.1-1 mbar
P47-250-M30-U-2m PiL	Filling level	300-2500 mm	<0.3 % from the measured value ±2 mm
PLW-R320-15M rinstrum	Mass	0-1500 kg	Resolution 500 g
Pt100 Kimo	Temperature	0-50°C	±0,3 % of the value ±0.25°C
Thermo-Hygro-Barometer PCE-THB38 PCE	Moisture of the air	10-95% r.h.	±3 % of the value ±3 % r.h.
Thermo-Hygro-Barometer PCE-THB38 PCE	Ambient pressure	1000-1100 hPa	±2 hPa

Table 1 Measuring devices used during the project

The pressure drops are measured with differential pressure sensors over different sections (heights) at the wall. The total pressure drop is composed of the pressure drop of 1 m height of the bed and an underlying screen. The empty pipe velocity is measured with hot-wire anemometers in the outlet pipe of the gas volume flow outside the construction. From this, the volume flow rate is determined. To improve the comparability of materials, the Reynolds number for bulk materials is used [8].

$$Re_{Schütt} = \frac{2}{3} \cdot \frac{\rho_F \cdot v_R \cdot x'_{ST}}{(1-\varepsilon) \cdot \eta_{fl}} \quad (8)$$

Here x'_{ST} is the Sauter diameter. The porosity ε and empty pipe velocity v_R are assumed to be uniformly distributed in radial and axial directions. The density ρ_F and dynamic viscosity η_{fl} of the air depend on the air temperature and pressure, which are recorded as described earlier.

Steady-state experiments

In Figure 7, the pressure drop over the dimensionless Reynolds number is shown.

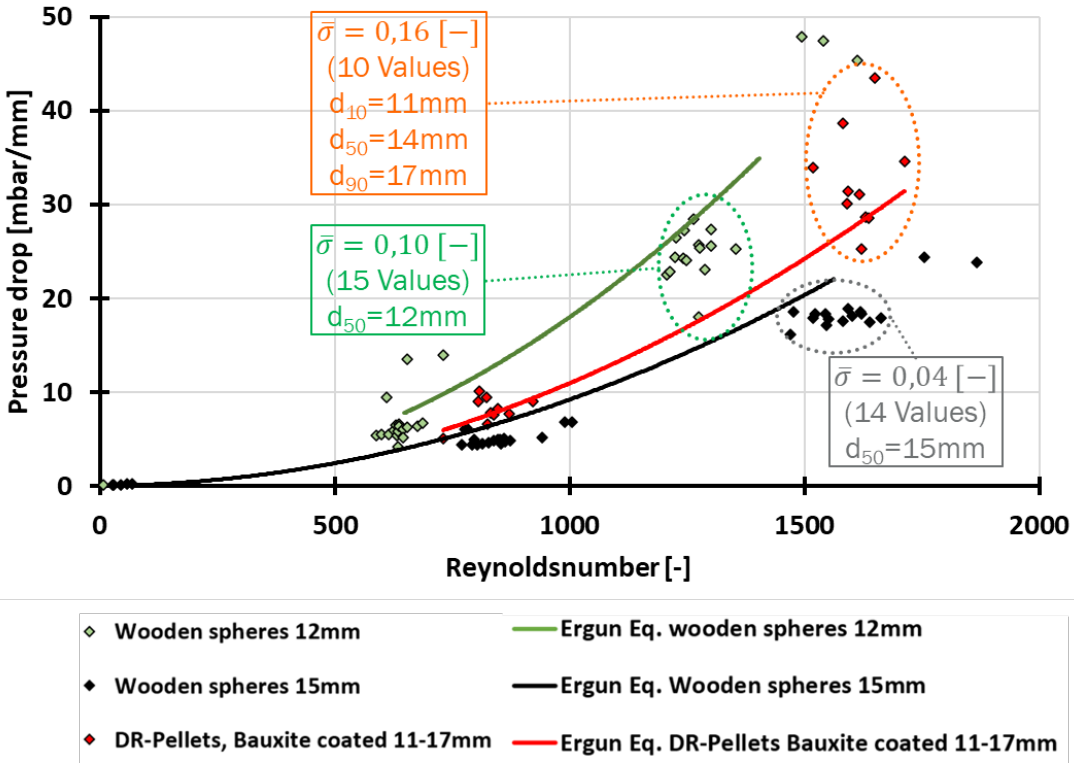

Figure 6: Pressure drops for the different sample materials in the test tube

The dots mark the measured values, while the lines represent the theoretical pressure drops per mm (for simplicity further on just called pressure drop) according to the equation of Ergun.

$$\frac{\Delta p}{H} = 150 \cdot \mu_F \cdot u_0 \frac{(1-\varepsilon)^2}{{d_{32}}^2 \cdot \varepsilon^3} + 1{,}75 \cdot \rho_F \cdot {u_0}^2 \cdot \frac{(1-\varepsilon)}{d_{32} \cdot \varepsilon^3} \tag{9}$$

As expected the smaller 12 mm wooden spheres have a higher pressure drop than the larger ones with a diameter of 15 mm. The measure values are a bit lower than the results from the Ergun equation. This may be related to the higher void volume near the walls. DR-Pellets have a broad size distribution compared to the consistent diameter of the wooden spheres. This results in a higher pressure drop compared to the 15 mm wooden spheres. The measured values are quite consistent with the Ergun equation, may be since wall effects and higher flow resistance due to the heterogeneous particle sizes compensate each other. The values measured for pellets also show a higher deviation of the pressure drop measurements of different experiments. This is most probably related to the heterogenous bulk properties resulting from the pellet size distribution. The Ergun equation uses an average (Sauter) diameter and neglects the size and shape distribution. This results in a theoretical curve below the measurements. These differences between theory and measurement give a first glimpse on root causes for heterogeneous conditions in industrial DR furnaces.

	Gas flow		*Pressure drop*	
	Mean value [m^3/h]	Standard deviation [-]	Mean value [mbar/m]	Standard deviation [-]
Wooden spheres 12 mm (37 experiments)	193	0.2385	6.6	0.4511
	401	0.0308	28.4	0.3019
Wooden spheres 15 mm (41 experiments)	216	0.4701	5.0	0.4177
	405	0.0617	18.7	0.1138
Bauxite coated DR-Pellets (20 experiments)	203	0.4841	8.1	0.4776
	395	0.0299	32.6	0.1555

Table 2 Mean values of the stationary experiments in the tubular rig

The outflow experiments were controlled by the opening width of the round gate opening. The first opening is the minimum usable opening width. If the opening is selected smaller, the respective material forms bridges and the outflow is blocked. For wooden spheres of 12 mm, this minimum opening is 80 mm, for wooden spheres of 15 mm diameter it is 90 mm and for the DR-Pellets 100 mm. The second width of the opening is 33 % wider. Figure 8 displays the dependency of the descent rate on the air velocity.

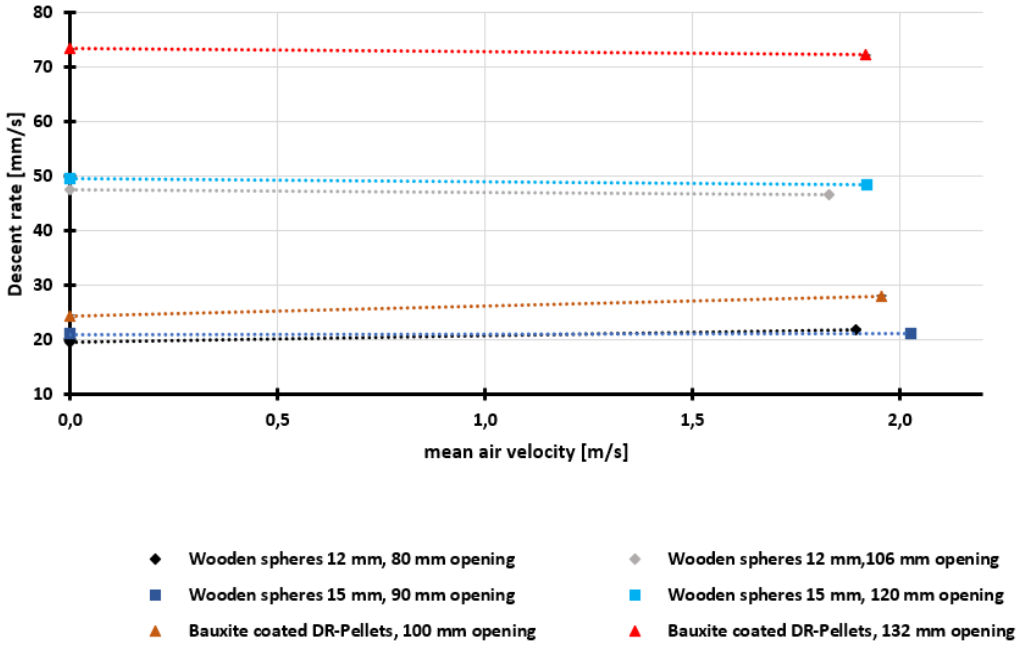

Figure 7: Mean descent rates for different slide openings in the test tube

At slower descent rates of all materials, the air flow partly increases the bulk descent rates. This may be explained by the air flow raising the particle mobility. For the larger openings, the air velocity tends to decrease the descent rate. This may be related to the counterflow of solid and air flow. However, the differences are small and may also be caused by statistic effects. The results are summarized in Table 3.

Material	Opening [mm]	Gas volume flow (Empty pipe) [m³/h]	Air velocity in bulk (calculated) [m/s]	Descent rate of particles (measured) [mm/s]	Particle mass flow (measured) [kg/s]
Wooden spheres 12mm	80	0	0	19.7	0.66
$\bar{T} = 23.8\ °C$	80	209	1.9	21.0	0.67
$\bar{p}_U = 1.003\ bar$	106	0	0	47.6	1.49
$\bar{\varphi}_{rel.} = 49.0\ \%$	106	202	1.8	46.7	1.28
Wooden spheres 15mm	90	0	0	21.1	0.70
$\bar{T} = 20.4\ °C$	90	213	2.0	21.2	0.67
$\bar{p}_U = 1.004\ bar$	120	0	0	49.6	1.50
$\bar{\varphi}_{rel.} = 403\ \%$	120	202	1.9	48.5	1.45
Bauxite coated DR-Pellets	100	0	0	24.3	3.42
$\bar{T} = 19.0\ °C$	100	209	2.0	28.1	4.19
$\bar{p}_U = 1.008\ bar$	132	0	0	73.4	10.3
$\bar{\varphi}_{rel.} = 41.1\ \%$	132	205	1.9	72.3	10.7

Table 3 Overview of experimental results of the outflow experiments

Dynamic experiments

In addition to the descent rate of the bulk and the respective pressure drop for the steady state experiments, the change of the pressure drop as a function of time during outflow is a decisive parameter. Therefore, in the following figures, the measured and calculated (Ergun equation) pressure drop is plotted over time. Figure 9 shows three diagrams. The first diagram shows the results for the wooden spheres with 12 mm, the second for the wooden spheres with a 15 mm diameter and the third one includes the results for DR-Pellets.

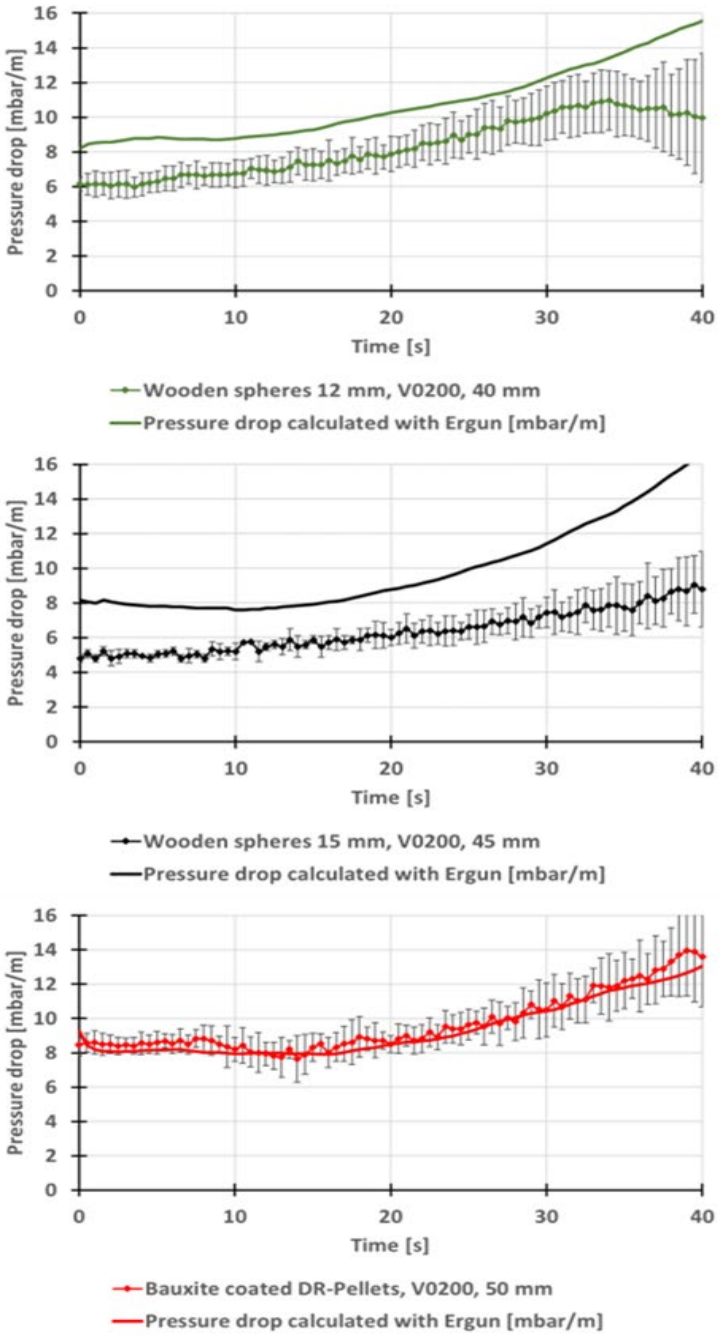

Figure 8: Measured and calculated pressure drop during the outflow of particles with counterflowing gas with 200 m^3/h

Similar to the stationary experiments, the theoretical calculation of the pressure drop of the wooden spheres is higher than the measured values. For the DR-Pellets, the calculated values fit the measurements.

3.3 Investigation of pressure drop in the tubular rig: Coupled DEM/CFD simulations

The simulations conducted to investigate the pressure drop in a tubular rig were designed to replicate the experimental conditions from BFI as closely as possible. The rig was modeled in the DEM code as well as in the computational fluid dynamics (CFD) environment (OpenFOAM). Pressure measurements were taken at five points along the height of the test tube wall under various flow rates and conditions.

The simulations were carried out for wooden spheres of 12 and 15 mm diameter, with gas volume flows of 200 m³/h and 400 m³/h (described in detail in Table 2). Key parameters such as ambient pressure, moisture content, and temperature were taken into account to ensure the accuracy of the simulation results.

Material	Sphere Diameter (mm)	Gas Flow (m³/h)	Gas Flow Standard Deviation	Pressure Drop (mbar/m)	Pressure Drop Standard Deviation
Wooden Spheres	12	193	0.2385	6.6	0.4511
Wooden Spheres	12	401	0.0308	28.4	0.3019
Wooden Spheres	15	216	0.4701	5	0.4177
Wooden Spheres	15	405	0.0617	18.7	0.1138

Table 4 Results from the experiments with wooden spheres

The simulation setup for the 15 mm wooden spheres is shown in detail in Figure 10. The DEM porosity field for the test tube shows the distribution of particles within the tube and their impact on the flow field.

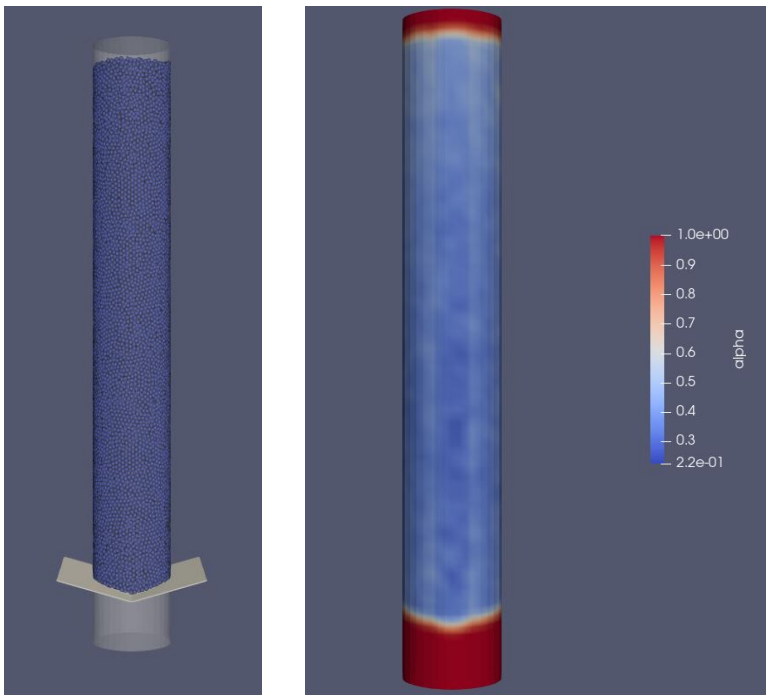

Figure 9: DEM simulation of the test tube filled with wooden spheres (left) and its respective porosity field (right)

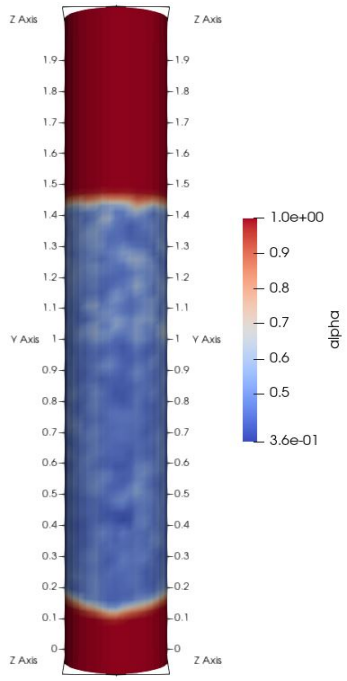

Pressure Drop Results

The simulation results for the pressure drop were compared with experimental data from BFI (experimental data) and RUB (simulation data). The pressure drop results are summarized in the table below (see Table 4 for corresponding trial conditions):

	BFI	RUB	
T12.1	660	722	[Pa/m]
T12.2	2840	3189	[Pa/m]
T15.1	500	596	[Pa/m]
T15.2	3260	3741	[Pa/m]

Table 5 Pressure drop for the experiments at BFI and respective simulations at RUB

Figure 10: DEM porosity field for the test tube filled with 15 mm wooden spheres

The pressure drop as a function of time for the dynamic experiments was also analyzed. The graph below shows the comparison of pressure/height calculations between the BFI experimental data and the simulation at RUB:

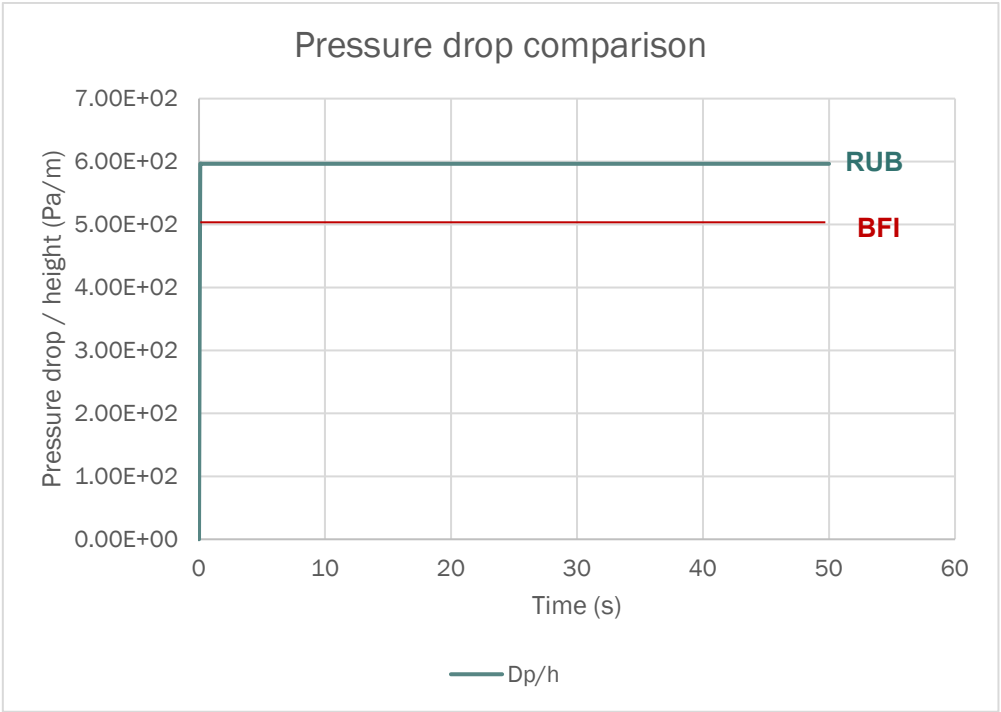

Figure 11: Pressure drop comparison for RUB and BFI for the 15 mm wooden spheres (3rd case at Table 4 above)

A comparison of pressure drop between the experiments and simulations revealed a deviation of approximately 20%. This is the same trend as for Figure 9, where BFI compared experiments against simple (non DEM/CFD) Ergun calculations. Further refinement of the calculation of the DEM porosity field (avoiding local discontunities by smoothening of porosity field) will be carried out for better agreement.

The pressure distribution in the test tube is also investigated, where 15 mm wooden spheres are used as the particles in the medium. The diagram on the right illustrates a vertical column with designated sections and specified pressure measurement points. The pressure measurement points are located at various heights within the column to capture the pressure profile accurately. The gas inlet is located at the bottom (0.12 meters from the base), and the gas outlet is at the top. The color-coded pressure distribution on the rightmost image shows the pressure gradient along the column, with a high-pressure zone at the bottom (near the gas inlet) and a lower pressure at the top (near the gas outlet). The pressure color scale ranges from approximately 99000 Pa to 100500 Pa.

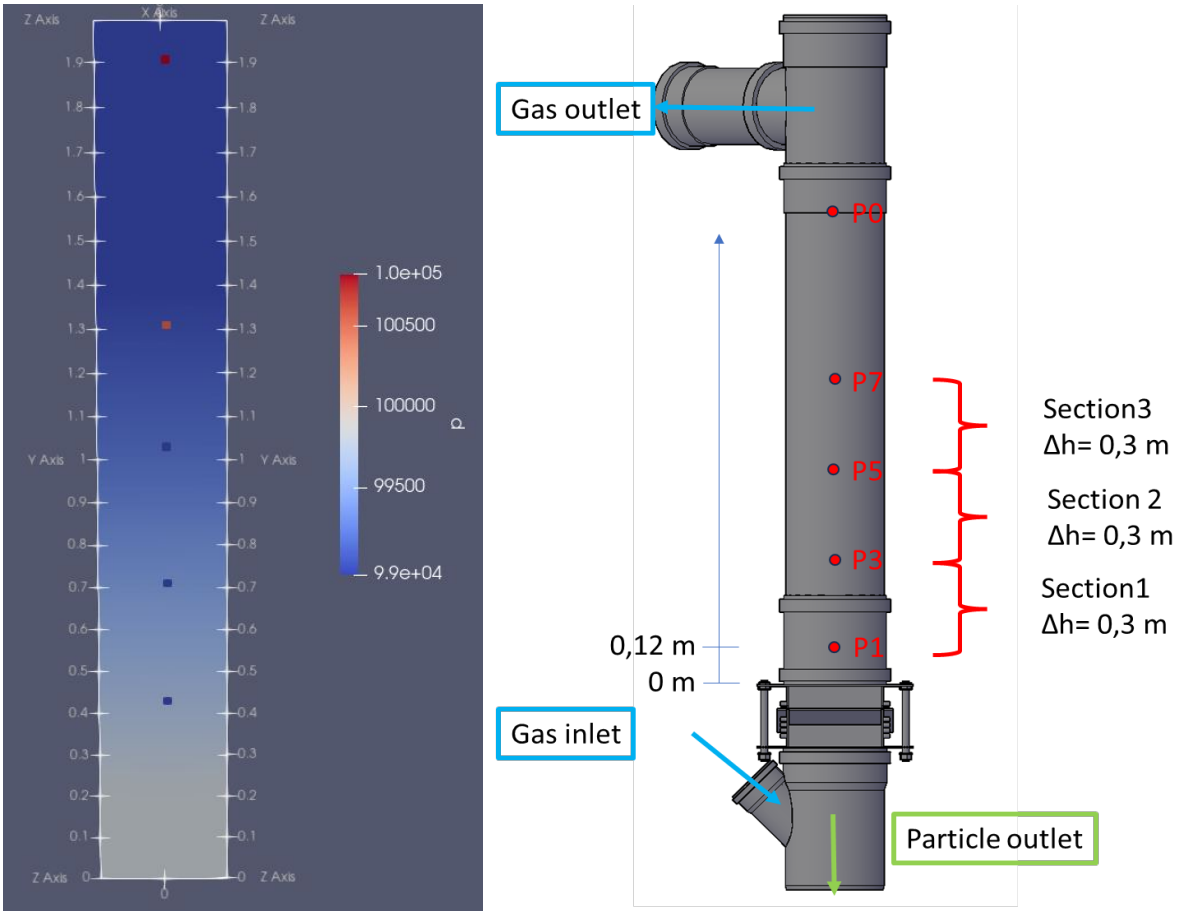

Figure 12: Pressure calculation at the five specified points: simulation (left) and design of experimental setup (right)

The graph below displays the pressure variation with height for the experiments at BFI and the simulations at RUB. For both conditions, there is a rapid decrease in pressure within the first 0.5 meters, indicating that most of the pressure drop occurs in the lower section of the column. Beyond 0.5 meters, the gradient of pressure decreases, indicating a more gradual reduction in pressure with height. Around the 1-meter height, the pressure stabilizes for both setups, with BFI and RUB pressures converging to approximately 98990 Pa and 99120 Pa, respectively.

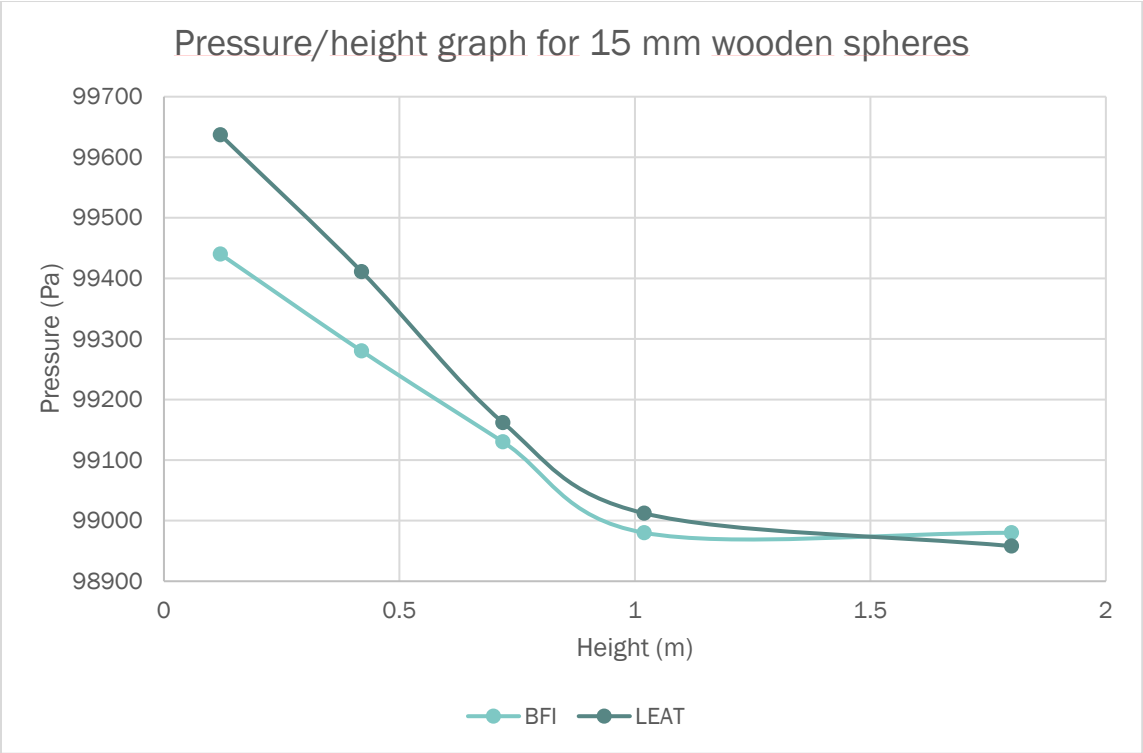

Figure 13: Pressure/height chart for simulation 3 (15 mm wooden spheres at the flow rate of 219 m^3/h)

The pressure/height graph and the vertical column simulation together provide a better understanding of the pressure behavior in the gas-solid flow system. There is a clear pressure gradient from the base to the top of the column, as expected in vertical flow systems.

3.4 Shaft simulations: pressure drop investigation for three test cases

The pressure-drop and outflow experiments described so far must be extrapolated to the process conditions and the geometry of the technical device aimed at. For this purpose, an analysis of a shaft furnace configured according to the Midrex geometry is conducted.

In this set of simulations, pellets move from the top downwards while air flows from the bottom of the shaft furnace. In order to reduce the computational effort, the particle shape is simplified to be spherical in most of the domain but better approximated in regions where required. This simplification is reasonable for DR since the fresh pellets coarsely resembles spheres. The radius of hematite (Fe_2O_3) pellets was set to 10 mm, no size distribution is considered here. Additionally, a simplification of the geometry is also required in order to achieve faster simulations. The full geometry is given at Figure 15 on the right and the simplification is shown in Figure 16 below.

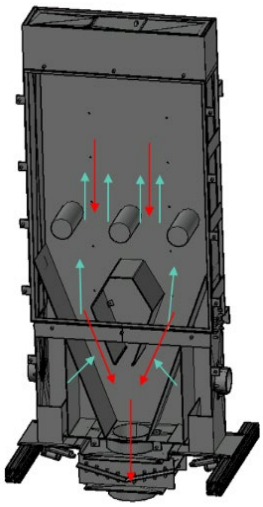

Figure 14: Midrex Geometry

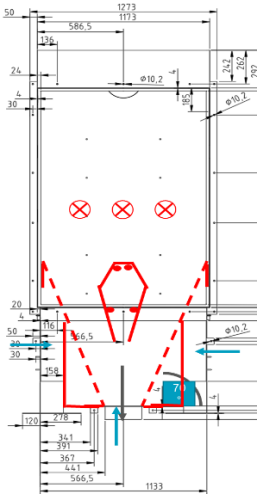

Figure 15: Simplified version of Midrex Geometry

The simplified version of the Midrex geometry has a height of 2.2 m and a similar version, displayed in Figure 17, has the additional 'Christmas tree' modification in the middle of the furnace.

Figure 16: BFI Shaft simplified version (left), BFI shaft with pellets inside (middle) and modification with the 'Christmas Tree' (right)

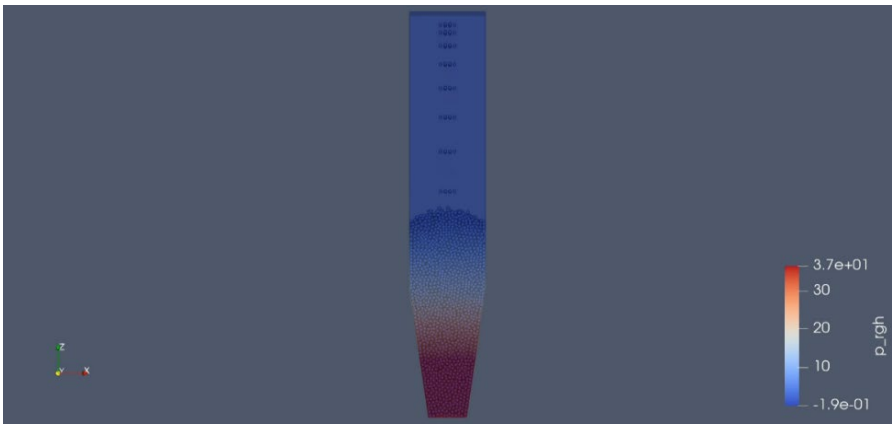

Figure 17: MIDREX Shaft Simulation for Test Case 1 with air flowing from the bottom and particles dropping from the top

The setup of the simulation is illustrated in Figure 18; the pellets are moving from the top downwards in uniform motion, while the gas is flowing from the bottom of the shaft furnace. This is only done for the 1st test case (dynamic simulations), as in test cases 2 and 3 the shaft furnace setup is initially filled with particles (steady-state simulations, no particle outflow) (see Figure 19).

Figure 18: MIDREX Shaft Simulation for Test Cases 2 and 3 with air flowing from the bottom and particles initially placed inside the shaft geometry

Test case 1 and test case 2 are done without the 'Christmas tree', while the third test case employs the 'Christmas tree' modification. The test cases and the results are described in detail below:

1. In test case 1, cold simulations (ambient temperature) are performed using two different gas compositions: air (77 mass % N_2 and 23 mass % O_2) and pure hydrogen (100%). Both simulations maintained a constant volume flow which was set at 0.15 m^3/h (this results in 2 m/s superficial velocity). The emphasis here was on determining pressure drop over the furnace's height under these varying gas compositions.

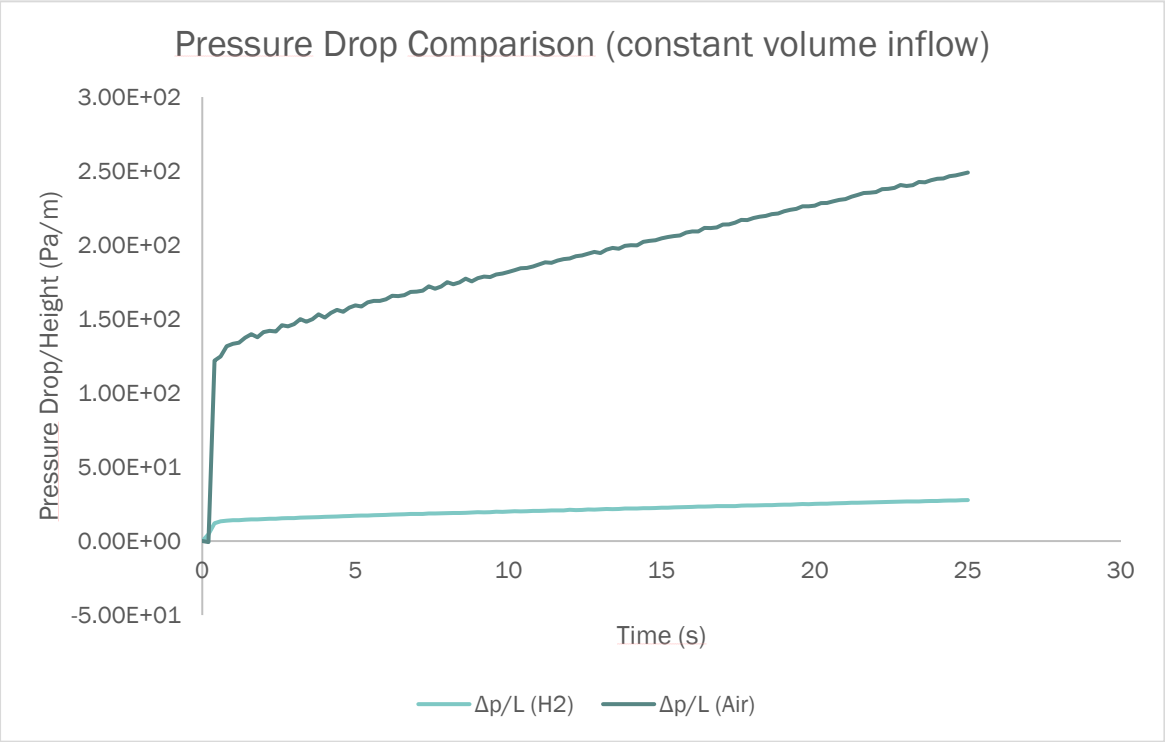

Figure 19: Pressure Drop Comparison (Constant Volume)

2. The second test case involves a comparison between air flow set at 0.1 m/s through the inlet and hydrogen flow at 2 m/s. Both scenarios maintained a constant mass for the fluid flow.

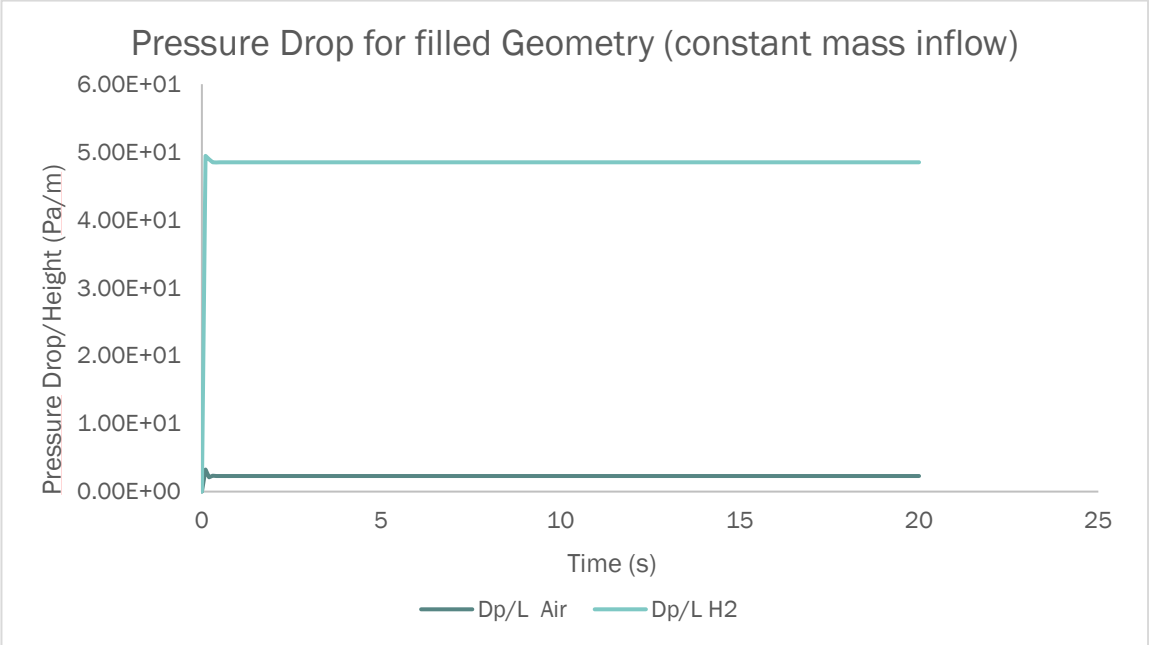

Figure 20: Pressure Drop Comparison (Constant Mass)

3. For the third test case, a modification was introduced to the shaft furnace model, akin to a 'Christmas tree' addition. The comparison focused on pressure drop/height using hydrogen for two geometries: with the added modification and without it.

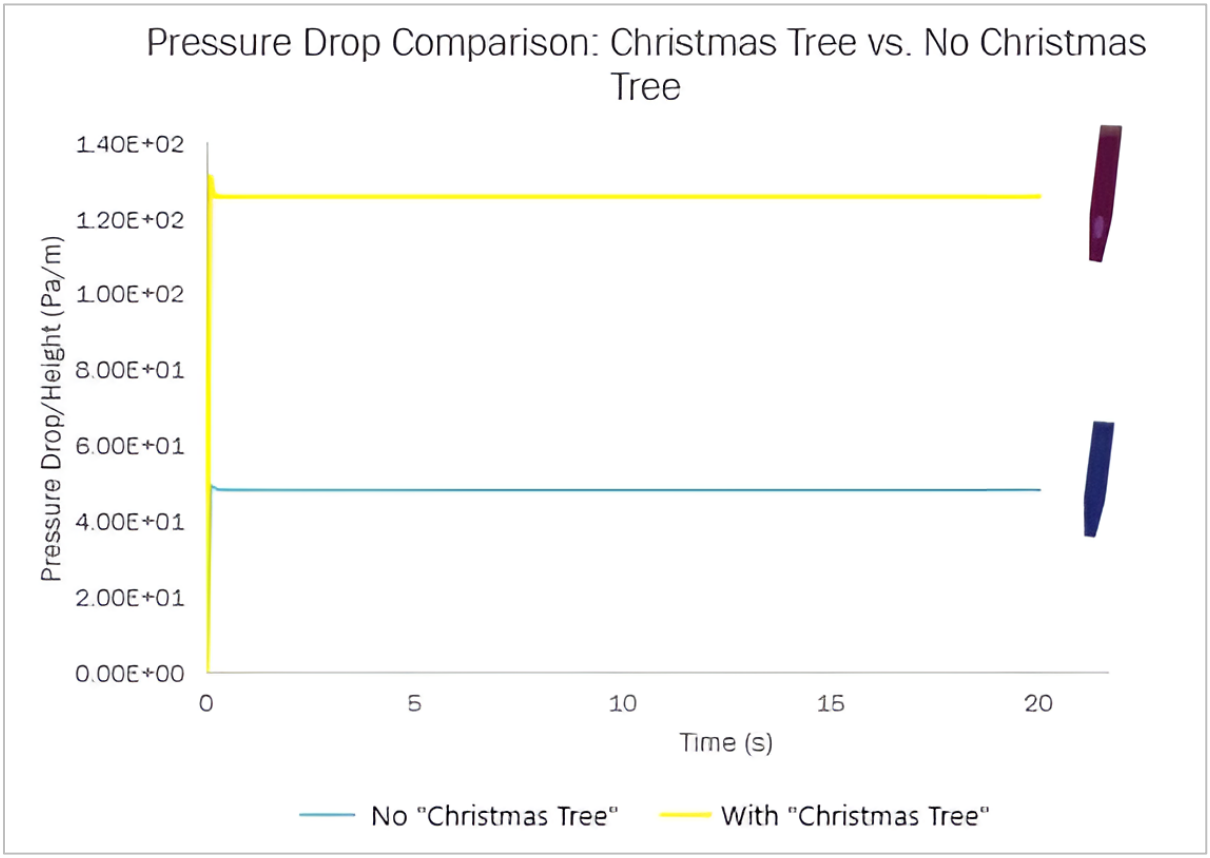

Figure 21: Pressure Drop Comparison: Christmas Tree (yellow) vs. No Christmas Tree (blue)

A short summary of the three test cases is presented below:

Test Case 1: As expected hydrogen shows lower pressure drop than air. Air is a mixture of gases, with a density of approximately 1.2 kg/m³ at standard conditions, while hydrogen is a single gas with a density of approximately 0.09 kg/m³ at the same conditions. Because of this difference in density, air has a higher momentum and kinetic energy than hydrogen, which results in a higher pressure drop as it flows around particles. In addition, air has a higher viscosity than hydrogen, which means it has a greater resistance to flow. This results in more energy being dissipated as frictional drops as the air flows around particles, further contributing to the higher pressure drop.

Test Case 2: The higher pressure drop observed for hydrogen can be attributed to its much higher velocity. Although hydrogen has lower density, viscosity, and thus lower resistance, the substantial increase in velocity introduces turbulence and increased frictional drops, ultimately contributing to the observed higher pressure drop in the hydrogen flow scenario.

Test Case 3: The increased pressure drop in the geometry with the 'Christmas tree' modification suggests that the added flow obstacle disrupts the gas flow dynamics within the furnace. The presence of the 'Christmas tree' reduces effective flow area in this region, separation, and eddies in the gas flow lead to increased velocity, friction and pressure drop compared to the unmodified geometry.

Next steps

The next step for this set of simulations is the replication of the solid and gas flow experiments from BFI with the new demo scale shaft furnace test rig, which is already constructed. The simulation setup at RUB is prepared and the experiments are expected to start at the end of this year.

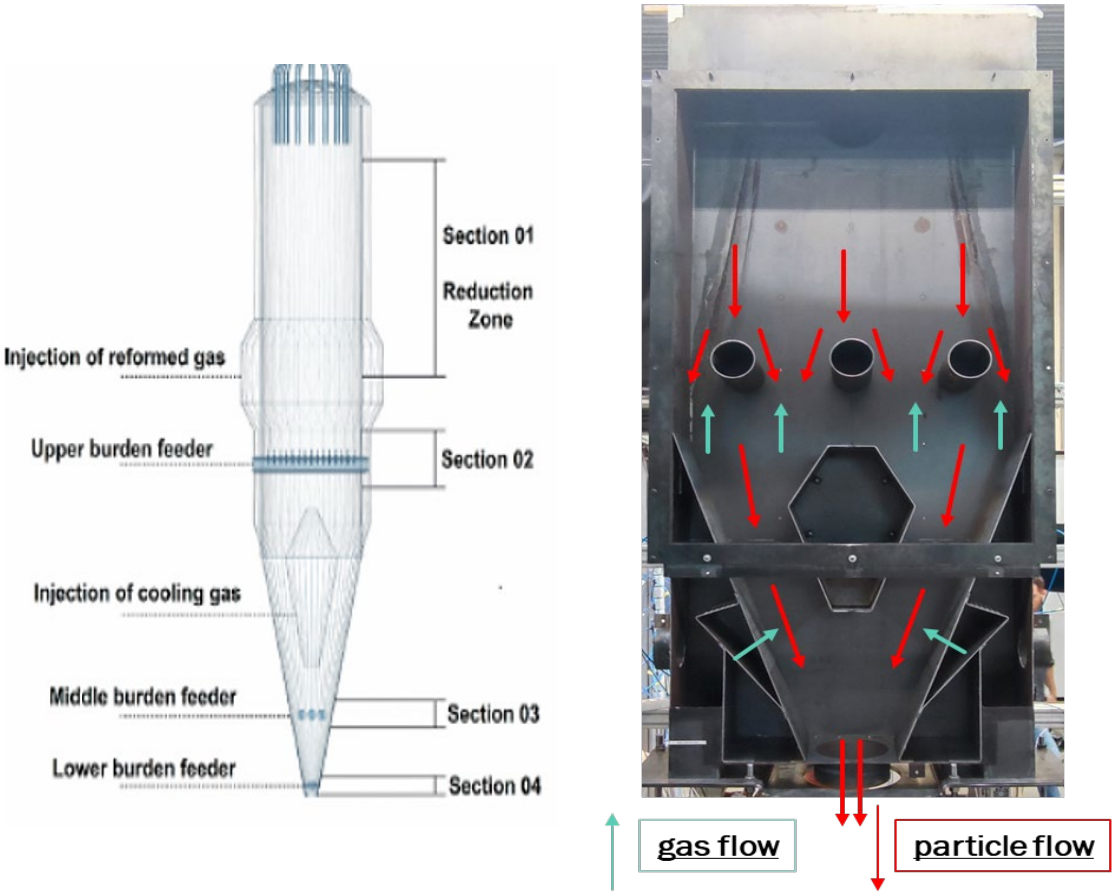

Figure 22: Picture of the demo scale shaft construction (right) based on the Midrex design (left)

4. Conclusion

The deliverable outlines the experimental setups and simulation methods used to understand the interaction between granular particles and gas flow, specifically in the context of the Direct Reduction Iron (DRI) process. A combination of DEM and CFD is used to simulate the behavior of iron ore pellets and wooden spheres and gas flow within a shaft furnace under various conditions.

Two main experimental setups were used: a tubular device and a shaft construction. The tubular device, with a vertical orientation and simple flow direction is used for preliminary tests. It features a diameter of 300 mm and a filling height of 1400 mm, with air flowing upwards through the material. Trials were performed with two sizes of wooden spheres and with iron ore pellets. The results show some deviations from Ergun calculations which however can be explained by the specific conditions like e.g. wall effects and grain size distribution. The pellet trials show significantly higher fluctuation, probably due to the different particles sizes resulting in heterogenous local bulk properties. This is a boundary conditions which is important for industrial DR shaft furnaces since flow heterogeneities are linked to reactions and temperature and can have impact on process stability and quality. The demo scale shaft furnace construction is more complex, allowing for internal installations and equipped with two inlets for gas flow. This setup will be used to track particle movement through an acrylic front plate, with various operational conditions.

For simulations, the DEM-CFD coupling routines combined DEM for particle motion with CFD for fluid dynamics, leveraging OpenFOAM for the latter. The simulations aimed to replicate momentum exchange in a counter-flow configuration, using simple spheres as particle models. Two volume flow rates, 100 and 200 m^3/h, were examined, and pressure drop measurements along the vertical axis were used to characterize the flow field. The agreement between the simulated and actual pressure drop confirms the effectiveness of these models in predicting granular flow behavior in silos.

The simulation results also offer a detailed understanding of the pressure dynamics in a vertical gas-solid flow system (tubular rig) using 15 mm wooden spheres. The comparative analysis of the BFI and RUB conditions reveals small differences of the pressure values and pressure drop gradients, suggesting variations in experimental parameters. The current model successfully captures the general trend of pressure drop observed experimentally but overpredicts its magnitude. This discrepancy highlights the need for further model refinement and validation. Potential sources of error include simplifications in particle interaction models, inaccuracies in input parameters, and limitations of the CFD-DEM coupling approach. By identifying critical regions of pressure variation and understanding the impact of different conditions, we can enhance the performance and effectiveness of gas-solid flow processes.

5. References

[1] Collaborative Research Centre (CRC) 287, https://bulk-reaction.de

[2] Projects B3, C3, C7 of: https://bulk-reaction.de/publications/

[3] Deshpande, R.; Mahiques, E.; Wirtz, S.; Scherer, V. (2022): "Resolving particle shape in DEM simulations from tabulated geometry information," Powder Technology, no. 407, p. 117700. DOI: 10.1016/j.powtec.2022.117700.

[4] Illana, E.; Qyteti, K.; Scharnowski, M.; Brömmer, M.; Wirtz, S.; Scherer, V. (2024): "Shape-changing particles for locally resolved particle geometry in DEM simulations," Particuology 89, pp. 185–190. DOI: 10.1016/j.partic.2023.11.003.

[5] B. Krause, B. Liedmann, J. Wiese, S. Wirtz, and V. Scherer, "Coupled three-dimensional DEM-CFD simulation of a lime shaft kiln - Calcination, particle movement and gas-phase flow-field," Chem. Eng. Sci., no. 134, pp. 834-849, 2015.

[6] F. Bambauer, S. Wirtz, V. Scherer, H. Bartusch, "Transient DEM-CFD simulation of solid and fluid flow in a three dimensional blast furnace model," Powder Technology, no. 334, pp. 53-64, 2018.

[7] Di Felice, R. (1994). The voidage function for fluid-particle interaction systems. International Journal of Multiphase Flow, 20(1), 153e159. https://doi.org/10.1016/0301-9322(94)90011-6

[8] S. Maaß, M. Kraume, "Determination of breakage rates using single drop experiments," Chem. Eng. Sci., Volume 70, 2012, pp. 146-164, https://doi.org/10.1016/j.ces.2011.08.027.